nanomaterials

MDPI

*Supplementary Materials*

# Self-Adaptive Flask-Like Nanomotors Based on $Fe_3O_4$ Nanoparticles to a Physiological PH

**Tianyu Gao [1], Jinwei Lin [2], Leilei Xu [1,*] and Jianguo Guan [1,2,*]**

[1] State Key Laboratory of Advanced Technology for Materials Synthesis and Processing, School of Materials Science and Engineering, Wuhan University of Technology, Wuhan 430070, China; gty@whut.edu.cn.
[2] State Key Laboratory of Advanced Technology for Materials Synthesis and Processing, International School of Materials Science and Engineering, Wuhan University of Technology, Wuhan 430070, China; linjinwei@whut.edu.cn.
* Correspondence: xull@whut.edu.cn (L.X.); guanjg@whut.edu.cn (J.G.)

**Supplementary Table:**

**Table S1.** Typical parameters used in the simulations.

| Parameters | Description | Values | Units |
|---|---|---|---|
| S_$Fe_3O_4$ * | surface molar concentration | $7.14\times10^{-5}$ | $mol/m^2$ |
| Zeta_flask | Zeta potential of FCNMs | -0.057 | V |
| D_H | diffusivity of $H^+$ | $9.31\times10^{-9}$ | $m^2/s$ |
| D_OH | diffusivity of $OH^-$ | $5.3\times10^{-9}$ | $m^2/s$ |
| D_• OH | diffusivity of • OH | $2.3\times10^{-9}$ | $m^2/s$ |
| D_$O_2$ | diffusivity of $O_2$ | $1.97\times10^{-9}$ | $m^2/s$ |
| D_$C_6H_8O_7$ | diffusivity of $C_6H_8O_7$ | $0.66\times10^{-9}$ | $m^2/s$ |
| D_$C_6H_7O_7$ | diffusivity of $C_6H_7O_7^-$ | $0.98\times10^{-9}$ | $m^2/s$ |

* Calculation of surface molar concentration of $Fe_3O_4$ NPs ($S_{Fe3O4}$)

From the TEM images (Figure 2b), it can be estimated that the average volume of individual flask-like carbonaceous carrier (FCC, only the carbon shell is counted, and the cavity is not counted) is $V_{FCC}= 2.76\times10^{-20}\ m^3$ and the internal surface area of individual FCC (only the bottom is counted, and the neck is not counted) is $S_{FCC} = 3.35\times10^{-13}\ m^2$.

Based on the density of amorphous carbon ($\rho_C=1.8\times10^6\ g\ m^{-3}$), the weight of individual FCC ($m_{FCC}$) is calculated as follows:

$$m_{FCC} = V_{FCC} \times \rho_C = 4.97 \times 10^{-14} g \quad (1)$$

Based on the results of TG analysis (Figure 2e) and the relative molecular weight of $Fe_3O_4$ NP ($Mr_{Fe3O4}$=231.54 g/mol), the number of FCCs ($N_{FCCs}$) and the molar amount of $Fe_3O_4$ NPs contained in each FCCs ($n_{Fe3O4}$) can be calculated as follows:

$$N_{FCCs} = \frac{m'_{FCCs}}{m_{FCC}} = 7.08 \times 10^{10} \quad (2)$$

$$n_{Fe3O4} = \frac{m_{Fe3O4}}{N_{FCCs} \times Mr_{Fe3O4}} = 2.39 \times 10^{-17}\ mol \quad (3)$$

Assuming that the $Fe_3O_4$ NPs is evenly distributed at the bottom of the bottle, the surface molar concentration of the $Fe_3O_4$ NPs ($S_{Fe3O4}$) can be calculated as follows:

$$S_{Fe3O4} = \frac{n_{Fe3O4}}{S_{FCC}} = 7.14 \times 10^{-5}\ mol/m^2 \quad (4)$$

**Table S2.** Average size, saturation magnetization (Ms) and relative peroxidase-like activity of as-prepared different $Fe_3O_4$@OA NPs.

| Samples | Average size (nm) | Ms (emu/g) | Relative activity (%) |
|---|---|---|---|
| MNP-1 | 4.62 | 33.9 | 97.5 |
| MNP-2(5) | 6.85 | 50.5 | 69.8 |
| MNP-3 | 7.37 | 59.1 | 60.0 |
| MNP-4 | 4.19 | 40.9 | 100 |
| MNP-6 | 7.73 | 61.7 | 59.9 |
| MNP-7 | 8.66 | 65.3 | 40.9 |
| MNP-8 | 2.94 | 7.02 | 28.4 |
| MNP-9 | 9.52 | 71.3 | 64.1 |
| MNP-10 | 6.91 | 54.5 | 68.5 |
| MNP-11 | 6.06 | 49.9 | 83.8 |

**Supplementary Figure:**

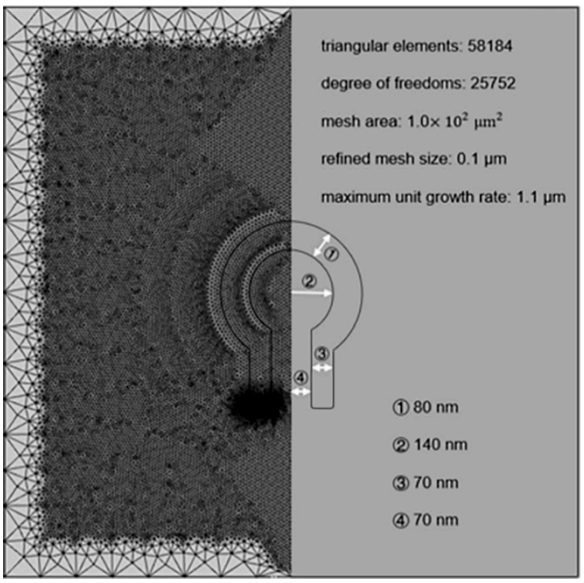


**Figure S1.** Meshing conditions of the theoretical model.

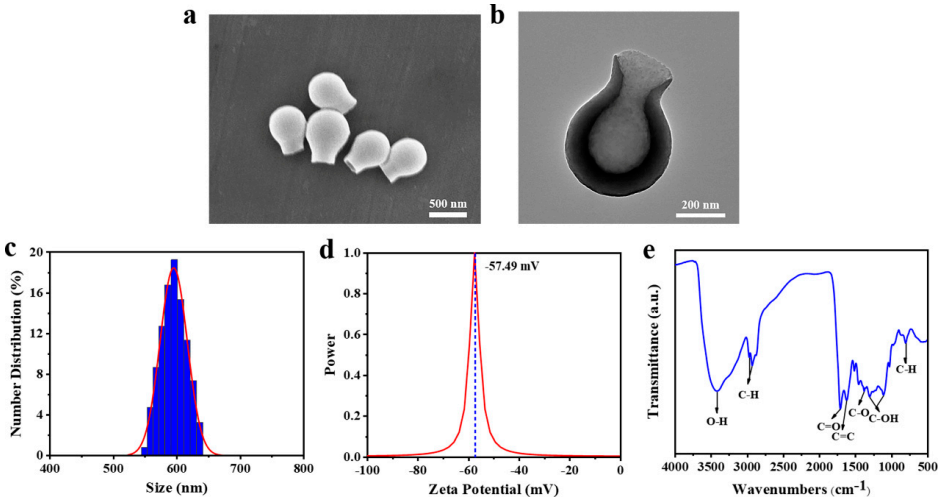


**Figure S2.** Characterizations of the FCCs. (**a**) SEM image of the FCCs. (**b**) TEM image of a typical FCC. (**c**) Zeta potential, (**d**) hydrodynamic size analysis and (e) FTIR spectra of the FCCs.

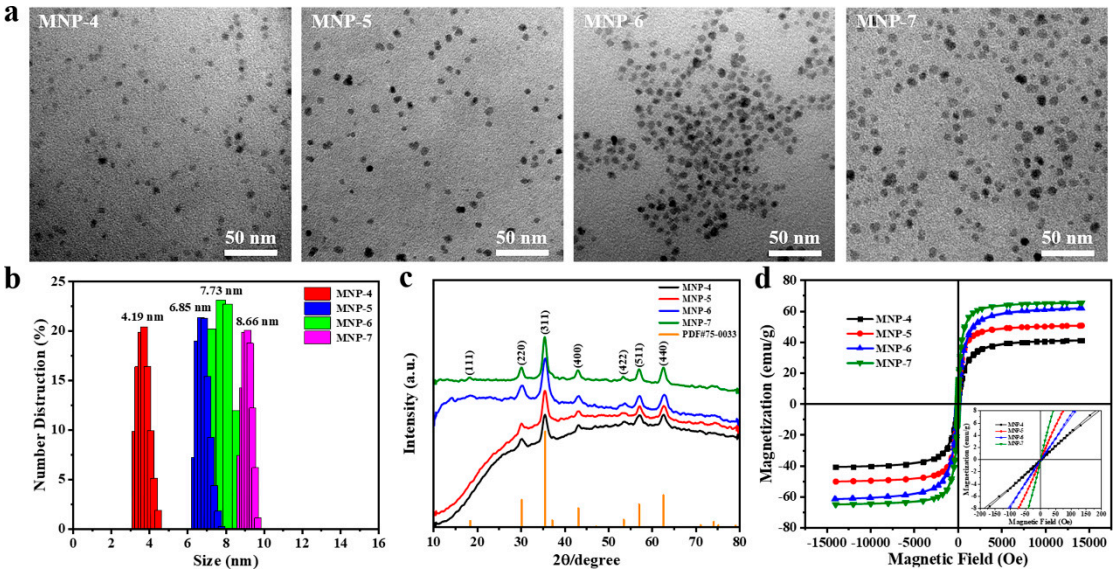


**Figure S3.** Characterizations of the $Fe_3O_4$@OA NPs synthesized at different aging temperatures (MNP-1, 200 °C; MNP-2, 220 °C; MNP-3, 240 °C). (**a**) TEM images, (**b**) hydrodynamic size analysis, (**c**) XRD patterns, and (**d**) hysteresis loops of the $Fe_3O_4$@OA NPs.

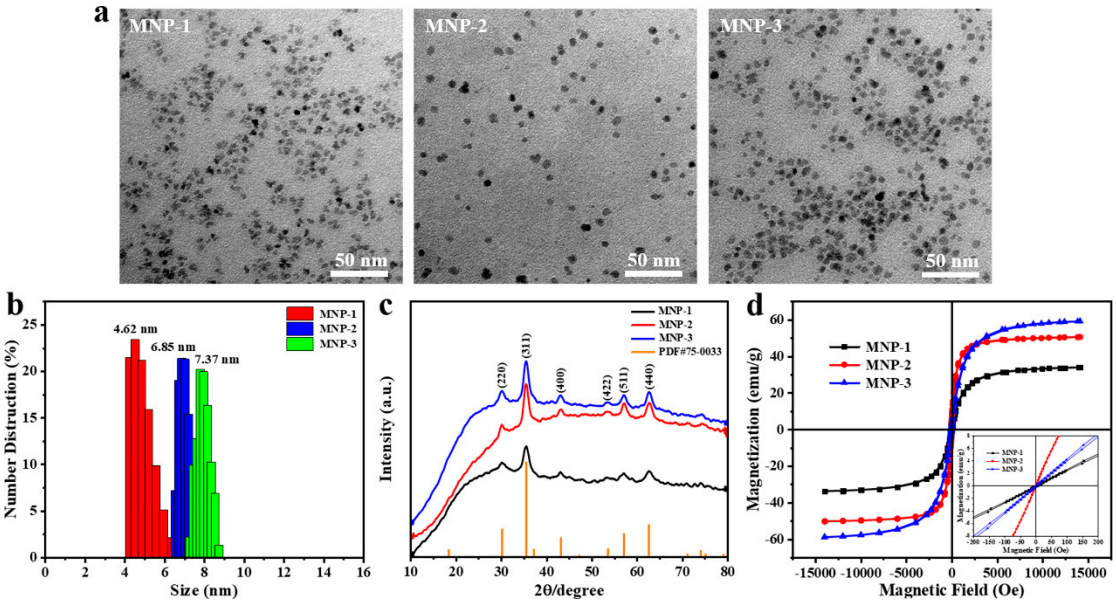


**Figure S4.** Characterizations of the $Fe_3O_4$@OA NPs synthesized at different aging time (MNP-4, 10 min; MNP-5, 30 min; MNP-6, 60 min; MNP-7, 90 min). (**a**) TEM images, (**b**) hydrodynamic size analysis, (**c**) XRD patterns, and (**d**) hysteresis loops of the $Fe_3O_4$@OA NPs.

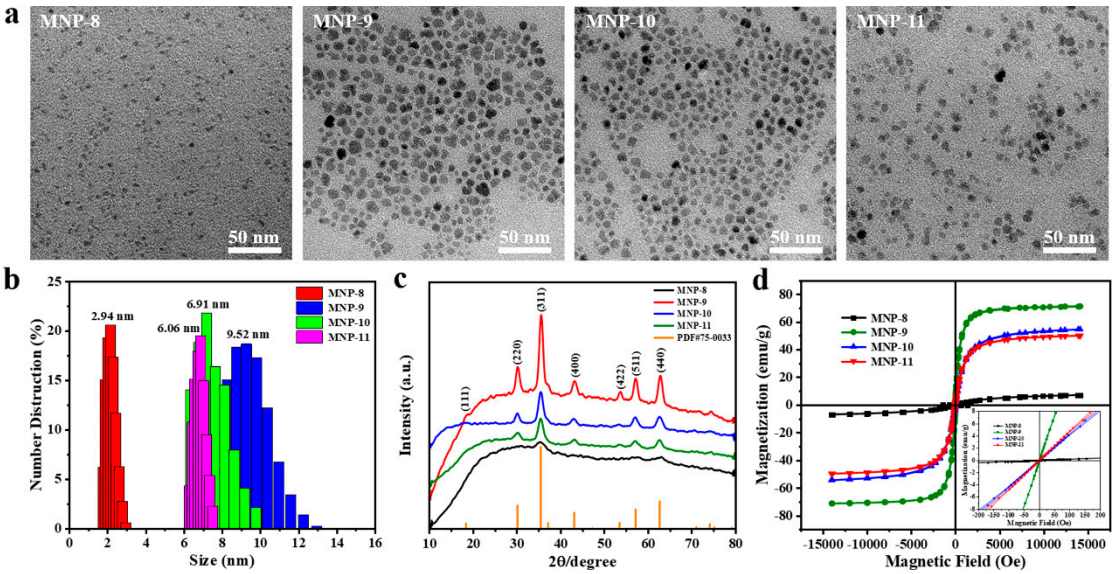


**Figure S5.** Characterizations of the $Fe_3O_4$@OA NPs synthesized at different raw material molar ratios between oleyl alcohol and oleic acid (MNP-8, 12 : 12; MNP-9, 16 : 8; MNP-10, 20 : 4; MNP-11, 24 : 0). (**a**) TEM images, (**b**) hydrodynamic size analysis, (**c**) XRD patterns, and (**d**) hysteresis loops of the $Fe_3O_4$@OA NPs.

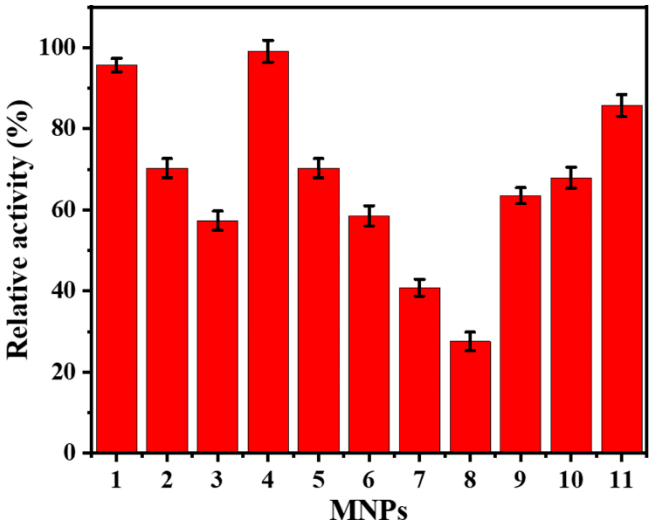


**Figure S6.** Relative peroxidase-like activities of the as-synthesized $Fe_3O_4$@OA NPs calculated by taking the group with the highest activity as 100%.

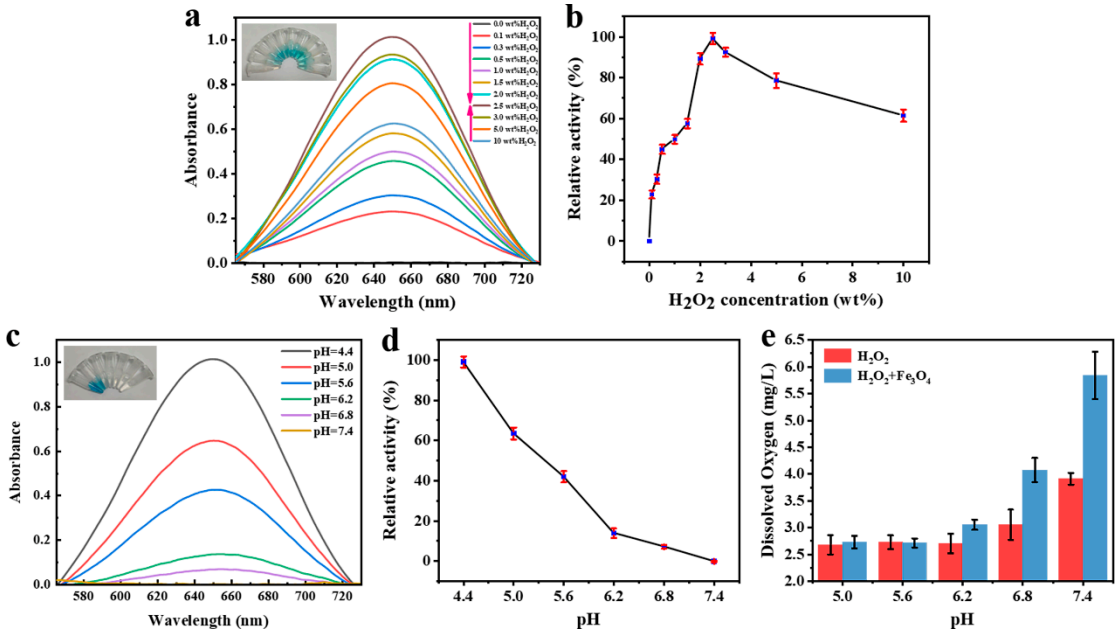


**Figure S7.** Characterizations of oil-soluble $Fe_3O_4$@OA and water-soluble $Fe_3O_4$@DMSA NPs. (**a**) TEM image of $Fe_3O_4$@DMSA NPs. (**b**) Fe 2p XPS spectra of the $Fe_3O_4$@DMSA NPs. (**c**) DLS, (**d**) VSM, and (**e**) FITR of $Fe_3O_4$@OA and $Fe_3O_4$@DMSA NPs. (**f**) Zeta potentials of the $Fe_3O_4$@DMSA NPs at different pH values.

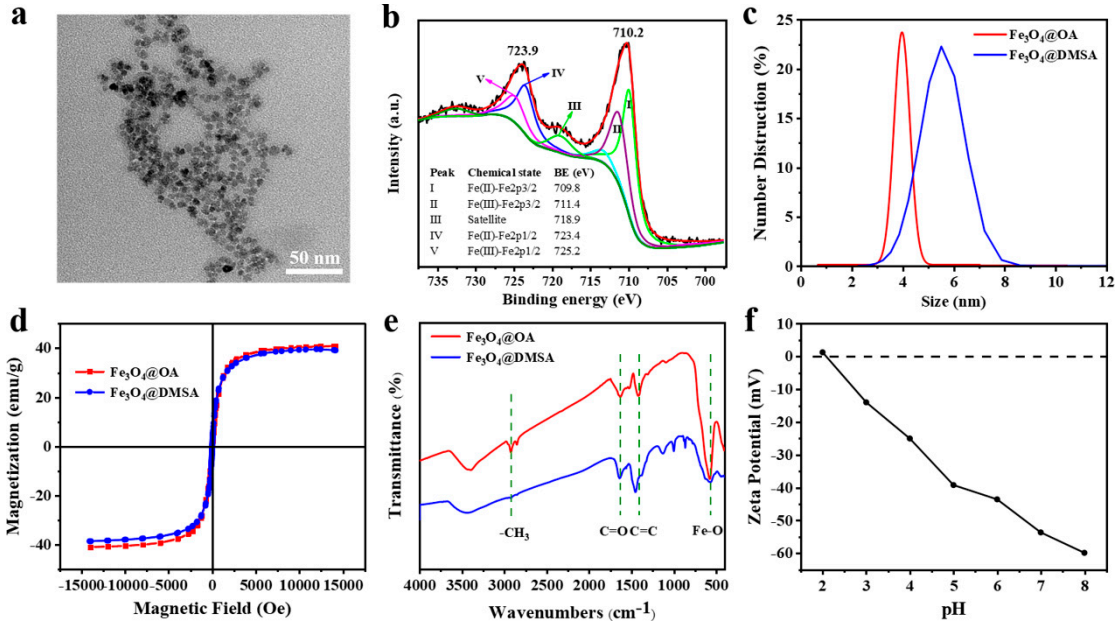


**Figure S8.** Verifications of dual enzyme-like activities of the $Fe_3O_4$@DMSA NPs. (**a**) UV-Vis spectra of the TMB-$H_2O_2$ system at different $H_2O_2$ concentrations. (**b**) Relative peroxidase-like activity of the $Fe_3O_4$@DMSA NPs at different $H_2O_2$ concentrations calculated by taking the activity at 2.5 wt% as 100%. (**c**) UV-Vis spectra of TMB-$H_2O_2$ system at different pH values. (**d**) Relative catalase-like activity of the $Fe_3O_4$@DMSA NPs at different pH values calculated by taking the activity at pH 7.4 as 100%. (**e**) Dissolved oxygen analysis of the as-prepared FCNMs moving in 2.5 wt% $H_2O_2$ aqueous solution at different pH values.

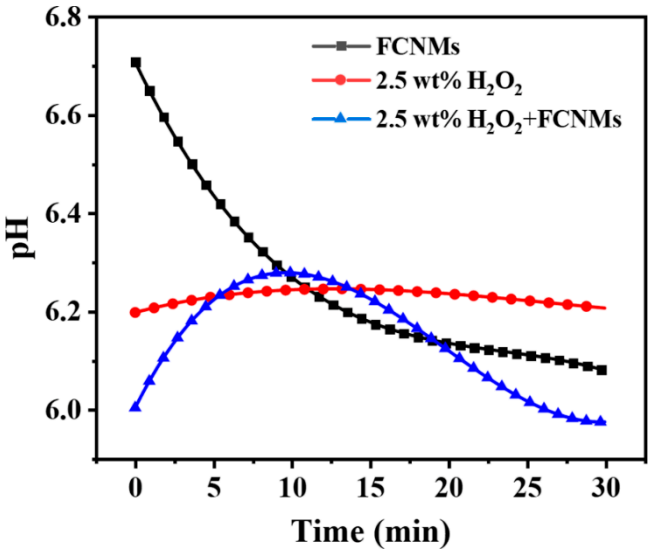


**Figure S9.** Verification of $OH^-$ product by monitoring the change of pH values of pure 2.5 wt% $H_2O_2$ aqueous solution, FCNMs aqueous solution and their mixed solutions in 30 min.

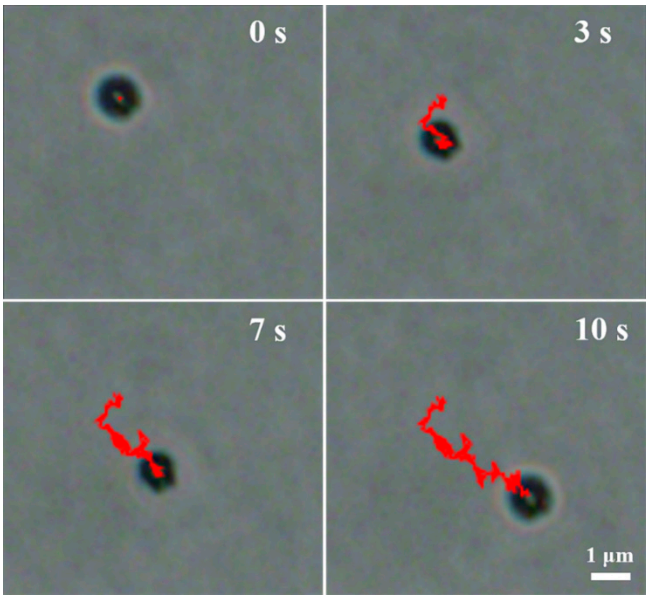


**Figure S10.** Time-lapse images monitored the motion direction of a comparable FCNM with a larger size of ~1 μm in 2.5 wt% $H_2O_2$ aqueous solution at pH 4.4.

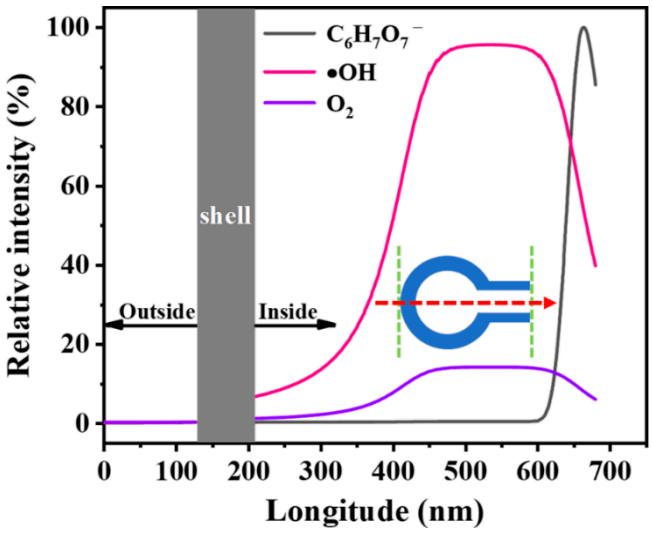


**Figure S11.** Concentration gradient distributions of •OH, $C_6H_7O_7^-$ and $O_2$ on the symmetric axis of the FCNMs.

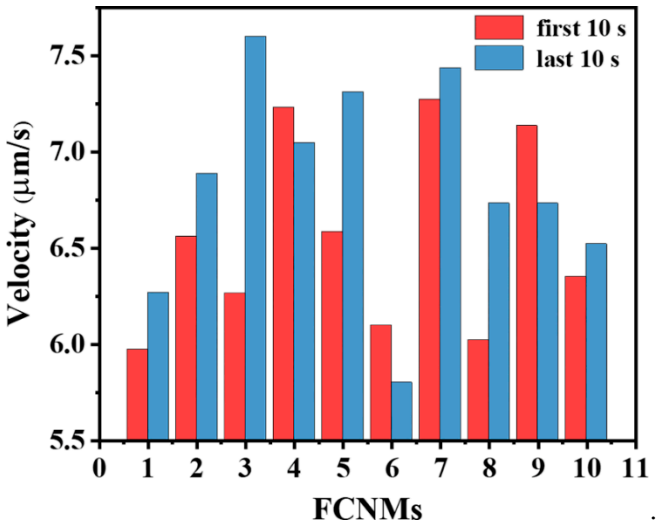


**Figure S12.** A discrete distribution of the average velocities of different chemotactic FCNMs in the first 10 s and last 10 s. .

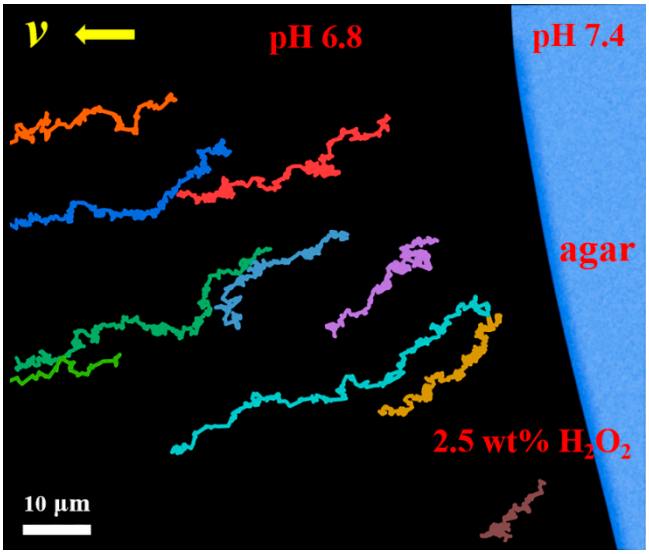


**Figure S13.** Chemotactic track trajectories of the FCNMs in 2.5 wt% $H_2O_2$ aqueous solution with a right-to-left gradually decreasing pH gradient in 30 s.

**Supplementary Video:**

**Video S1.** The FCNM moving in 0 wt% $H_2O_2$ aqueous solution.

**Video S2.** The FCNM moving in 2.5 wt% $H_2O_2$ aqueous solution at pH 5.6.

**Video S3.** The FCNM moving in 2.5 wt% $H_2O_2$ aqueous solution at pH 6.8.

**Video S4.** The FCNM with a larger size moving in 2.5 wt% $H_2O_2$ aqueous solution at pH 4.4 for observing its motion direction.

**Video S5.** The FCNM moving in 2.5 wt% $H_2O_2$ aqueous solution.

**Video S6.** The FCNMs moving in 2.5 wt% $H_2O_2$ aqueous solution with a left-to-right gradually decreasing pH gradient.

**Video S7.** The FCNMs moving in 2.5 wt% $H_2O_2$ aqueous solution with a right-to-left gradually decreasing pH gradient.